Clinical Anatomy 16:494–500 (2003)

ORIGINAL COMMUNICATION

Comparison of Mandibular Landmarks from Computed Tomography and 3D Digitizer Data

FRANK L'ENGLE WILLIAMS[1,2*] AND JOAN T. RICHTSMEIER[1,3]

[1]*Department of Anthropology, Pennsylvania State University, University Park, Pennsylvania*
[2]*Department of Anthropology and Geography, Georgia State University, Atlanta, Georgia*
[3]*Center for Craniofacial Development and Disorders, The Johns Hopkins Medical Institutions, Baltimore, Maryland*

We recorded 3D coordinates for 28 mandibular landmarks from three-dimensional reconstructions of CT axial slices using the image analysis program eTDIPS. The images were acquired from a pediatric series of human mandibles (neonate to 13 years of age) from the Bosma collection (Shapiro and Richtsmeier, 1997, Am. J. Phys. Anthropol. 103:415–416). To test the accuracy of these coordinate data, we recorded the same 28 landmarks directly on the Bosma mandibles using a Polhemus 3Space digitizer. The directly digitized landmarks serve as a gold standard upon which to evaluate the eTDIPS data. Standard deviations of landmark placement using eTDIPS show a greater degree of variation compared to the data gathered using the digitizer, although this error is more heavily concentrated in certain types of landmarks. All possible linear distances between unique pairs of landmarks were calculated, and like linear distances were compared between the two data collection methods. The absolute difference for all like linear distances ranged from 0.001–3.9 mm (mean = 0.377 mm; SD = 1.136), with the eTDIPS data being consistently larger than the digitizer coordinates. This study demonstrates that landmark coordinate data can be reliably collected from digital CT images of the human mandible. We define a set of mandibular landmarks useful in evaluating the effects of craniofacial disorders, growth and other biological processes. Clin. Anat. 16:494–500, 2003. © 2003 Wiley-Liss, Inc.

Key words: mandible; 3D reconstruction; digitization; measurement error

INTRODUCTION

As part of the craniofacial complex, the mandible not only transmits force to the rest of the skull via mastication, but also reflects general cranial growth patterns influenced by suture ossification, dental maturation, and splanchnocranium development. The mandible also reflects abnormal growth of the skull (Richtsmeier et al., 2000) and thus may be affected by, or play a causative role in, a variety of craniofacial disorders ranging from craniosynostosis to cleft palate (Cohen and MacLean, 2000). One way to address the relationship of these disorders to the mandible is to use landmark coordinate data and geometric morphometric methods. To do so, it is necessary to evaluate a set of landmarks that can be accurately obtained and precisely reproduced.

The protocol we define here utilizes computed tomographic (CT) images. CT data and skeletal reconstructions of the images have a wide range of applications for clinical and basic scientific research. CT data have been used to plan surgical procedures (Vannier et al., 1984; Leboucq et al., 1991; Fernbach and Feinstein, 1992), for postoperative evaluation (DeLeon et al., 2001), and to compare pathologic conditions to normal (Richtsmeier et al., 1998; Zumpano et al., 1999). Analysis of CT images has also played an important role in paleoanthropology (Zollikofer et al., 1995; Seidler et al., 1997; Conroy et al., 1998; Thompson and Illerhaus, 1998). The efficacy of CT images in capturing the true form of an object has been tested for the cranium (Hildebold and Vannier, 1988; Richtsmeier et al., 1995).

Grant sponsor: NIH; Grant number: P60 DE13078.

*Correspondence to: Frank L'Engle Williams, Department of Anthropology and Geography, Georgia State University, 33 Gilmer Street, Atlanta, GA 30303. E-mail: frankwilliams@gsu.edu

Received 20 January 2002; Revised 30 July 2002

Published online in Wiley InterScience (www.interscience.wiley.com). DOI 10.1002/ca.10095

Validation of the accuracy of mandibular measurements using CT images is difficult because, in contrast to the cranium, the mandible lacks a large number of foramina and other readily identifiable biological structures to use as landmarks.

We defined 28 landmarks and collected data directly from the mandibles and indirectly from CT images of the mandibles. We studied the distribution of error along all axes, both within and across techniques, and specific to each landmark to identify problematic axes and landmarks. We also compared all possible interlandmark distances obtained for each data collection technique to evaluate whether the same information (unique linear distances) is captured using image analysis on the one hand and a 3D digitizer on the other.

MATERIALS AND METHODS

We selected 22 mandibles from the Bosma collection (Shapiro and Richtsmeier, 1997), currently housed in the Department of Anthropology at the Pennsylvania State University. The Bosma collection is an undocumented sample of juvenile skulls ranging from perinatal ages to approximately 13 years. Each mandible was affixed to a Polhemus 3Space tabletop digitizer (Polhemus, Colchester, VT), subjected previously to accuracy (Hildebolt and Vannier, 1988) and repeatability tests (Corner et al., 1992), using plasticine to prohibit movement during and between landmarking trials. Inhibiting movement during data collection is absolutely necessary to acquire valid information about the relative location of landmarks. Preventing movement between landmarking trials of a single specimen avoids the necessity of translating and rotating the object to account for differences in orientation (Valeri et al., 1998; Lele and Richtsmeier, 2001). Landmark coordinate data were collected three times from each specimen. The three trials were conducted sequentially to create the most reliable estimates for each landmark location.

The Bosma mandibles were scanned using a GE CT9800 scanner at the Department of Neuroradiology, The Johns Hopkins Hospital. The research protocol for these CT scans has been previously described (Valeri et al., 1998). The x-, y-, and z-axes are internal to each CT study and are generated at the time the scans are acquired. Whole skulls were positioned in the CT scanner as a patient would be, with occiput against the examining table. Consequently, when viewing the image data, the x- and y-axes are the pixel rows and columns within each axial slice. The z-axis is determined by slice thickness and by the interpolation function of the software used in reconstruction.

We chose eTDIPS (Exploratory Two/Three Dimensional Image Processing System) to examine our CT images, create reconstructions, and collect landmark data. There are currently a number of image analysis programs available to researchers; we chose eTDIPS because of the quality of its reconstructions and its built-in landmarking tool (Mullick et al., 1999). This image analysis program uses a Win 2000/NT/x9 interface for visualizing and analyzing 3D images, and is available at no cost from the NIH Clinical Imaging Processing homepage (http://www.cc.nih.gov/cip/software/etdips/). Reconstructions can be easily rotated in all directions and viewed in their entirety, or partially, to enhance visualization and analysis of all external and internal surfaces and volumes.

CT slice images were stacked within eTDIPS by specifying x-, y- (pixel size), and z- (slice thickness) volume dimensions. A 3D surface reconstruction for each specimen was created using a chosen density threshold that corresponds to the Hounsfield unit scale (Spoor et al., 2000). Surface extraction thresholds, which need to be stipulated to produce a reconstruction, were determined empirically and typically consisted of 806 as the start threshold, and 3,155 as the end threshold. These thresholds were chosen to show the maximum amount of bony tissue with the least amount of distortion. The reconstructions, in conjunction with the axial slice images, were used to identify landmark locations using the eTDIPS landmarking tool interface. Landmark locations on each mandible were recorded twice using eTDIPS. The absence of a time interval between trials provided the most reliable estimate of landmark location and minimized intra-specimen error for this data collection technique.

Twenty-eight mandibular landmarks were selected to capture the shape of the mental region, body, and outer dimensions of the ramus. Because of the difficulty in obtaining true anatomical landmarks on the mandible, several of the landmarks we chose are "fuzzy," meaning that the definition of the landmark is larger than a single point within the observers' range of view (Valeri et al., 1998). Other landmarks are "constructed," meaning that their location is determined by constructing a line tangent to another landmark or bony edge (Bookstein, 1991). To locate a constructed landmark an anatomical feature, or "anchor," must be identified. In our data collection protocol, skulls were positioned in the appropriate plane (e.g., Frankfurt horizontal for landmarks on the sagittal plane) and constructed landmarks were located by departing in the appro-

TABLE 1. Description of Mandibular Landmarks Examined

Landmark name	Abbreviation (Number)[b]	Description	Type
Gnathion	GNA (1)	Most anteroinferior point on mental symphysis	Fuzzy
Pogonion	POG (2)	Most anterior projection of bone on mental symphysis	Fuzzy
Infradentale	INFR (3)	Most central point on mandibular alveolus	Biological
Mental foramen[a]	MEN (4)	Anteromedial edge	Biological
Alveolar border of body[a]	ALV (5)	Directly above mental foramen	Constructed
Inferior border of body[a]	IBB (6)	Directly below mental foramen	Constructed
Gonion[a]	GON (7, 22)	Junction of ramus and inferior border of body	Constructed
Inferior posterior ramus[a]	PGA (8, 21)	Junction of gonial angle and posterior border of ramus	Constructed
Lateral mandibular condyle[a]	LAT (9, 17)	Most superolateral point on mandibular condyle	Fuzzy
Posterior mandibular condyle[a]	PSC (10, 18)	Most posterosuperior point on mandibular condyle	Fuzzy
Medial mandibular condyle[a]	MC (11, 19)	Most mediosuperior point on mandibular condyle	Fuzzy
Coronoid process[a]	COR (12)	Superior aspect	Biological
Superior anterior ramus[a]	SA (13)	Most anterior projection on anterior border of ramus	Fuzzy
Inferior anterior ramus[a]	AJUNC (14)	Junction of anterior border of ramus and alveolus	Fuzzy
Mandibular foramen[a]	MFO (15, 20)	Most inferior aspect	Biological
Superior mental spine	MSPIN (16)	Most superior aspect	Biological

[a]Indicates both right and left sides were landmarked.
[b]These are the numbers listed in Figures 1A, B. Landmarks with two numbers have both right and left sides depicted on Figures 1A, B.

priate directions from their anatomical anchors. We expected to find more error in fuzzy and constructed landmarks than in "biological" landmarks that are located on the basis of anatomy. We hypothesized that biological landmarks will have less error than constructed and fuzzy landmarks because biological landmarks (i.e., foramina, bony processes, and muscle insertions) are less subject to intra- and interobserver interpretation of placement criteria. Of the 16 landmarks listed in Table 1, seven are fuzzy, four are constructed, and five are biological. Figures 1a and 1b show the anatomical locations of these landmarks.

To compare the error generated by the two techniques of data collection, we first averaged the three trials of the 3Space digitizer and the two trials of eTDIPS for each of the 22 specimens to construct x-, y-, z-mean coordinates per landmark location for each of the techniques (x_1, y_1, z_1 and x_2, y_2, z_2).[1] For each specimen within each data collection technique, we compared each trial's coordinate to its average coordinate by taking the sum of the square root of the squared differences between each trial and its mean, and dividing this sum by the number of trials,

$$\frac{\sum \sqrt{(x_i - \bar{x}_i)^2}}{n}$$

where x_i = each trial's coordinate for a landmark along each axis, $\bar{x}_i$ = the mean coordinate of each landmark for each axis, and n = the number of trials (three for the digitizer data and two for the eTDIPS data). This procedure was done for all landmarks, for all three axes and both techniques. The resulting 28×3 matrix for each specimen is the average difference from the mean difference along each axis. This approach eliminated differences due to coordinate systems within the data and allowed for the comparison of error between the two data collection techniques. Standard deviations of landmark placement were obtained for each coordinate per landmark along each axis using all individuals in the sample (n = 22; see Table 2). Separate t-tests were conducted to determine whether the distribution of error along a given axis was significantly different from other axes within each technique and from like axes between techniques.

Euclidean Distance Matrix Analysis (EDMA) was used to calculate the difference between the linear distances obtained using the 3Space digitizer and those captured using eTDIPS (Lele and Richtsmeier, 2001). We then calculated the mean difference (n = 22 specimens) between the two techniques for all 378 linear distances. By comparing the absolute difference between the two data collection techniques, we were

[1]Different numbers of trials for 3Space and eTDIPS does not lead to an artificially lower standard deviation for the 3Space data. The average standard deviation for all 3Space trials is 0.241 (minimum = 0.000; maximum = 0.559). Removal of one of the 3Space trials did not substantially affect the results. The larger number of trials for 3Space was meant to provide a stringent gold standard test for eTDIPS.

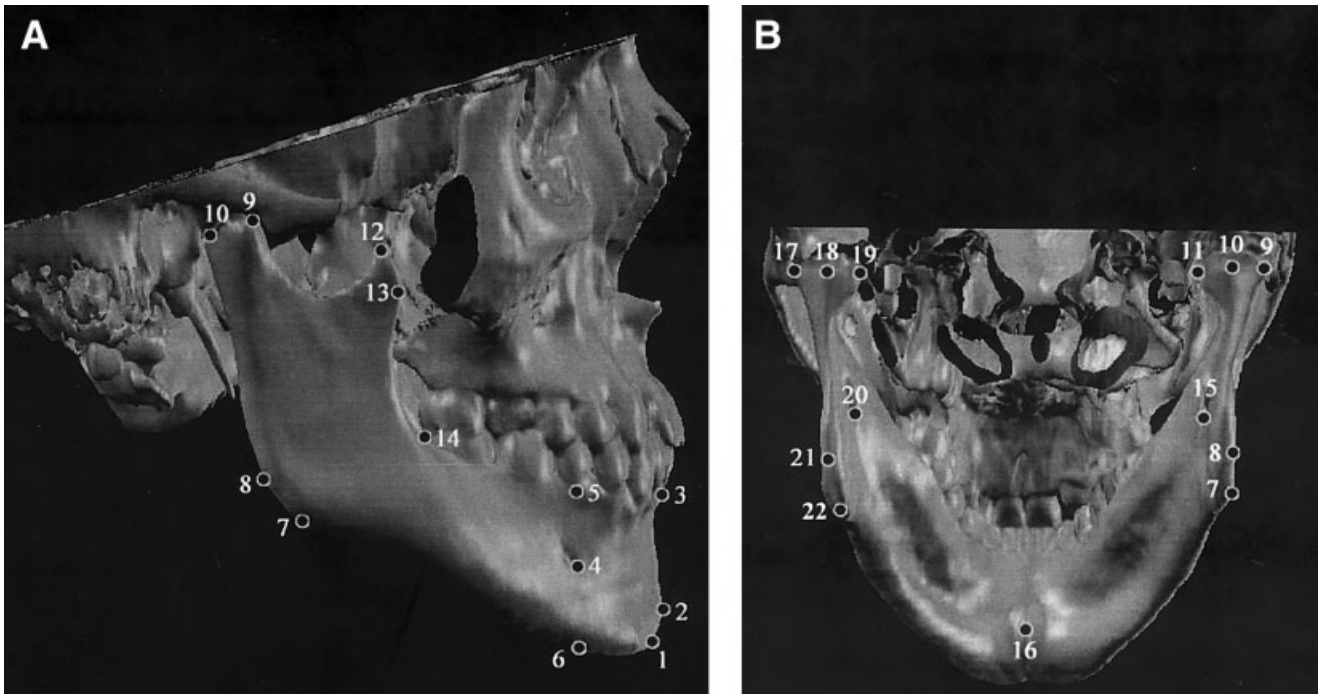

Fig. 1. **A:** Lateral view of the mandible showing the anatomical position of the landmarks used in this study. Each landmark is represented by a number: 1, gnathion; 2, pogion; 3, infradentale; 4, mental foramen; 5, alveolar border of body; 6, inferior border of body; 7, gonion; 8, inferior posterior ramus; 9, lateral mandibular condyle; 10, posterior mandibular condyle; 12, coronoid process; 13, superior anterior ramus; 14, inferior anterior ramus (see Table 1 for descriptions). **B:** Lingual view of the mandible showing the anatomical position of the landmarks used in this study. Each landmark is represented by a number (see Table 1 for descriptions). Right and left sides of the same landmark are given different numbers. The right-sided landmark numbers correspond to those illustrated in Figure 1A except for 11, medial mandibular condyle, and 15, mandibular foramen; 16, superior mental spine; 17, lateral mandibular condyle; 18, posterior mandibular condyle; 19, medial mandibular condyle; 20, mandibular foramen; 21, inferior posterior ramus; 22, gonion. The landmarks are labeled on eTDIPS reconstructions, rather than photographs, to demonstrate the quality of our images.

able to evaluate the validity of images for our image analysis and data collection protocol.

RESULTS

Consistency of Landmark Placement

The magnitude of error local to each landmark obtained using the 3Space digitizer is frequently similar to that exhibited by landmarks obtained using eTDIPS (Table 2), but *t*-tests between corresponding axes of the two techniques show a significant statistical difference between the degree of error for each digitizer axis and its eTDIPS counterpart (Table 3). The SDs of landmark placement in eTDIPS are significantly greater along each axis than those exhibited by the 3Space digitizer data. The landmarks that are responsible for the statistical differences between each eTDIPS axis and its digitizer counterpart are primarily constructed landmarks, such as gonion (GON) and the alveolar border above the mental foramen (ALV), and fuzzy landmarks such as the superoanterior ramus (SA) and the junction of the alveolus and ramus (AJUNC).

We carried out *t*-tests of the SDs of landmark placement within each of the techniques to determine whether a particular axis within the eTDIPS or 3Space trials exhibited more error than the other axes. For the 3Space digitizer trials, error along the *z*-axis is statistically greater than along the *x*- and *y*-axes (Table 4). The greater error along the *z*-axis occurs most frequently for landmarks located on the ramus (the *z*-axis is tracking the superoinferior axis of landmark locations).

In eTDIPS, the *y*- and *z*-axes (anteroposterior and superoinferior, respectively) contain more error than does the *x*-axis (mediolateral). In fact, a relatively large degree of error on the *z*-axis is often associated with a concomitant large error on the *y*-axis for the same landmarks. This arises from difficulties in locating landmarks that are fuzzy, which could have a number of possible locations differing only slightly in anteroposterior or superoinferior positions (many of the

TABLE 2. Standard Deviations of Landmark Coordinates Using the 3Space Digitizer and eTDIPS[a]

	3Space			eTDIPS		
Landmark	*x*	*y*	*z*	*x*	*y*	*z*
GNA	0.254	0.246	0.223	0.233	0.420	0.220
POG	0.131	0.157	0.219	0.190	0.245	0.462
INFR	0.078	0.145	0.188	0.178	0.323	0.373
R-MEN	0.118	0.128	0.179	0.222	0.313	0.354
R-ALV	0.268	0.188	0.314	0.508	0.500	0.672
R-IBB	0.241	0.422	0.297	0.403	0.397	0.238
L-MEN	0.124	0.119	0.127	0.266	0.482	0.394
L-ALV	0.331	0.424	0.151	0.275	0.449	0.253
L-IBB	0.228	0.269	0.392	0.521	0.499	0.188
R-GON	0.305	0.314	0.362	0.299	0.591	0.360
R-PGA	0.365	0.274	0.490	0.358	0.198	0.589
R-LAT	0.213	0.167	0.259	0.288	0.426	0.671
R-PSC	0.232	0.187	0.279	0.565	0.321	0.778
R-MC	0.156	0.181	0.255	0.385	0.370	0.451
R-COR	0.167	0.226	0.492	0.241	0.316	0.165
R-SA	0.236	0.181	0.299	0.898	1.352	0.783
R-AJUNC	0.433	0.539	0.559	0.301	0.396	0.644
L-GON	0.410	0.391	0.235	0.611	0.380	0.497
L-PGA	0.366	0.201	0.340	0.233	0.353	0.510
L-LAT	0.183	0.105	0.246	0.213	0.318	0.496
L-PSC	0.144	0.195	0.351	0.493	0.366	0.959
L-MC	0.199	0.177	0.445	0.285	0.313	0.371
L-COR	0.222	0.135	0.206	0.195	0.240	0.159
L-SA	0.326	0.178	0.401	0.312	0.182	0.695
L-AJUNC	0.310	0.163	0.302	0.373	0.649	0.964
R-MFO	0.333	0.353	0.338	0.358	0.420	0.764
L-MFO	0.256	0.193	0.296	0.279	0.530	0.390
MSPIN	0.134	0.201	0.217	0.319	0.284	0.684

[a]R, right side; L, left side. Abbreviations for landmarks are defined in Table 1. Values are SD in mm.

fuzzy landmark categories in our study are on the midline of the mandible such as the gnathion and pogonion [Fig. 1a], or the midpoint of a bony projection such as the posterosuperior condyle [Fig. 1a,b]; these landmarks may be less prone to error in the mediolateral plane). Additionally, the *z*-axis in eTDIPS may have poorer resolution than the *x*- and *y*-axes because of the necessary interpolation function used in 3D reconstruction. This may account for some of the generally greater standard deviations per landmark location along the *z*-axis compared to the *x*-axis (Table 2; see Richtsmeier et al., 1995 for discussion).

Absolute Difference Between the Two Techniques

To assess the information contained within all three axes simultaneously, and to determine whether we obtained the same information using the two techniques, we calculated all possible interlandmark distances for the 3Space digitizer and for the eTDIPS data and obtained the absolute differences by subtracting one from the other. The 378 linear distances range in length from 4.882–82.741 mm. The correlation between the length of the linear distance and the mean absolute difference between the two data collection techniques is poor ($r^2 = 0.104$). The absolute difference between the 3Space digitizer data and the eTDIPS data, with respect to each linear distance, ranges from 0.001–3.889 mm (mean = 0.377 mm; SD = 1.136). Roughly one-third, or 33% of these differences are <0.5 mm, 58% are <1.0 mm, 91% are <2 mm, and 98% are <3 mm. The linear distances with the highest difference between techniques include those measures involving constructed and fuzzy landmarks (Table 1). Distances that have endpoints noted to be difficult to locate using eTDIPS are also associated with large absolute differences between

TABLE 3. Results of *t*-Tests Comparing Like Axes of the Two Data Collection Techniques

Axes compared	*t*-Test results
X (eTDIPS) and X (3Space)	$P = 0.003$; eTDIPS > 3Space
Y (eTDIPS) and Y (3Space)	$P = 0.000$; eTDIPS > 3Space
Z (eTDIPS) and Z (3Space)	$P = 0.000$; eTDIPS > 3Space

TABLE 4. Results of *t*-Tests Comparing Each Axis to All Others Within Each Data Collection Technique[a]

Axes compared	3Space digitizer	eTDIPS
X and Y	NS	$P = 0.036$; Y > X
Y and Z	$P = 0.007$; Z > X	NS
X and Z	$P = 0.004$; Z > Y	$P = 0.002$; Z > X

[a]NS, not significant; $P>0.05$.

the two techniques; for example, the medial mandibular condyle (MC) is partially obscured from view by the overlying mating surface of the glenoid fossa (Fig. 1b). The distance between two problematic landmarks combined the error local to each, producing a relatively large difference between the two techniques (Table 2).

Our biological landmarks exhibit the smallest difference between the two data collection techniques. These landmarks include the mandibular (MFO) and mental (MEN) foramina, as well as bony projections such as the coronoid process (COR); however, eTDIPS linear distances involving the superior mental spine (MSPIN) tend to differ more from their 3Space counterparts than do other distances that incorporate biological landmarks because muscle insertions are generally more difficult to locate on axial images than on the bones themselves.

The linear distances derived from eTDIPS landmark coordinate data tend to be larger than our 3Space digitizer data. Nearly two-thirds (62%) of the 378 linear distances in eTDIPS are slightly larger (from 0.001–3.889 mm) than the same linear distances in the 3Space digitizer data. Those linear distances that are larger in eTDIPS are predominantly associated with constructed and fuzzy landmarks (e.g., junction of alveolus and ramus [AJUNC], superior anterior ramus [SA], and inferior border of body [IBB]) that are more difficult to locate on CT reconstructions and axial slices (where pixilation decreases gradually) than on the mandibles themselves. The difficulty in locating these landmarks may be due to the operator's choice of a threshold value in eTDIPS where the amount of visible bony tissue can differ from the amount of real bone present.

DISCUSSION

Our results suggest that the coordinate data collected directly from the mandibles using the 3Space digitizer are more precise than similar data collected from images of the same mandibles using eTDIPS. Our results are consistent with other studies comparing anatomical and CT measurements (Corner et al., 1992; Richtsmeier et al., 1995; Valeri et al., 1998; Şenol et al., 2001). Valeri et al. (1998) reported lower standard deviations for landmark placement (1.15 mm for 30 trials and 0.75 mm for the last 10 trials alone) with a digitizer compared to those obtained using an image analysis program. Richtsmeier et al. (1995) found the absolute difference between cranial landmarks digitized using a 3Space digitizer and using CT axial slices to be between 1.13 and 2.37 mm. Nearly two-thirds of the absolute differences reported here are smaller than the lower boundary of error (1.13 mm) obtained by Richtsmeier et al. (1995). Our data may have a lower absolute difference between 3Space and image analysis data sets because we used both axial slices and 3D reconstructions to locate landmarks. Surface reconstructions, if used in conjunction with axial slices, increase the accuracy of collecting 3D coordinate data from images. Additionally, the use of 3D reconstructions increases the number of potential landmarks available.

Our data demonstrate that constructed and fuzzy landmarks generally exhibit relatively more error than biological landmarks. An important exception may be those biological landmarks that concern muscle insertions, such as the superior mental spine (MSPIN). The resolution necessary for muscle attachments to appear on CT reconstructions and axial images is only rarely available. Our linear distances that involve the superior mental spine tend to have more error than one would expect for biological landmarks.

The density threshold used in reconstructing an image from a series of axial slices also plays a role in the production of error. For example, 3D reconstructions can be a source of error when the landmark is located on an area of bone that is less dense than adjacent areas. Moreover, if landmarks are taken on a reconstruction with low density and then a higher density surface is reconstructed, the landmarks will be partially obscured by the newly reconstructed image because more pixels have taken on the density of bone and the previous landmarks are buried under the new surface. The user's choice of a threshold for surface reconstructions needs to be considered in any study attempting to extract data from CT images.

CT images have wide application to problems in craniofacial biology as they provide a nondestructive means of examining internal structures on fossil and bone. The landmarks acquired from such images can be used to infer how biological structures like the mandible respond to, and influence, craniofacial form. Although certain landmark types are easier to capture and reproduce than others, the landmarks examined here all have acceptable measures of error and may assist researchers investigating the effects of craniofacial disorders on the mandible.

ACKNOWLEDGMENTS

We would like to thank D. Kreger and V. DeLeon for their comments concerning measurement error and research design, and K. Aldridge for editing earlier drafts of this article. E. Lindsay skillfully prepared Figure 1. EDMA software is available at http://oshima.anthro.psu.edu.

REFERENCES

Bookstein FL. 1991. Morphometric tools for landmark data. New York: Cambridge University Press. 455 p.

Cohen MM, MacLean RE. 2000. Craniosynostosis: diagnosis, evaluation, and management. 2nd Ed. New York: Oxford University Press. p 1–454.

Conroy GC, Weber GW, Seidler H, Tobias PV, Kane A, Brunsden B. 1998. Endocranial capacity in an early hominid cranium from Sterkfontein, South Africa. Science 280:1730–1731.

Corner BD, Lele S, Richtsmeier JT. 1992. Measuring precision of three-dimensional landmark data. J Quant Anthropol 3:347–359.

DeLeon VB, Zumpano MP, Richtsmeier JT. 2001. The effect of neurocranial surgery on basicranial morphology in isolated sagittal craniosynostosis. Cleft Palate Craniofac J 38: 134–146.

Fernbach SK, Feinstein KA. 1991. The deformed petrous bone: a new plain film sign of premature lambdoid synostosis. Am J Roentgenol 156:1215–1217.

Hildebolt CF, Vannier MW. 1988. Three-dimensional measurement accuracy of skull surface landmarks. Am J Phys Anthropol 76:497–509.

Leboucq N, Montoya P, Martinez Y, Castan Ph. 1991. Value of 3D imaging for the study of craniofacial malformations in children. J Neuroradiol 18:225–239.

Lele SR, Richtsmeier JT. 2001. An invariant approach to statistical analysis of shapes: interdisciplinary statistics. London: Chapman & Hall CRC. 328 p.

Mullick R, Warusavithana SV, Shalini V, Pang P. 1999. "Plug-ins: a software model for biomedical imaging and visualization research." Biomedical Imaging Symposium: visualizing the future of biology and medicine, NIH. http://www.cc.nih.gov/cip/software/etdips .

Richtsmeier JT, Baxter LL, Reeves RH. 2000. Parallels of craniofacial maldevelopment in Down syndrome and Ts65Dn mice. Dev Dyn 217:137–145.

Richtsmeier JT, Cole TM, Krovitz G, Valeri C, Lele S. 1998. Preoperative morphology and development in sagittal synostosis. J Craniofac Genet Dev Biol 18:64–78.

Richtsmeier JT, Paik CH, Elfert PC, Cole TM, Dahlman HR. 1995. Precision, repeatability, and validation of the localization of cranial landmarks using computed tomography scans. Cleft Palate-Craniofac J 32:217–227.

Seidler H, Falk D, Stringer C, Wilfing H, Mueller G, Zur Nedden D, Weber G, Recheis W, Arsuaga JL. 1997. A comparative study of stereolithographically modelled skulls of Petralona and Broken Hill: implications for future studies of middle Pleistocene hominid evolution. J Hum Evol 33:691–703.

Şenol U, Çubuk M, Sindel M, Yildirim F, Yilmaz S, Özkaynak C, Lüleci E. 2001. Anteroposterior diameter of the vertebral canal in cervical region: comparison of anatomical, computed tomographic, and plain film measurements. Clin Anat 14:15–18.

Shapiro D, Richtsmeier JT. 1997. Brief communication: a sample of pediatric skulls available for study. Am J Phys Anthropol 103:415–416.

Spoor F, Jeffery N, Zonneveld F. 2000. Imaging skeletal growth and evolution. In: O'Higgins P, editor. Development, growth and evolution. London: The Linnaean Society of London. p 123–161.

Thompson JL, Illerhaus B. 1998. A new reconstruction of the Le Moustier 1 skull and investigation of internal structures using 3D-μCT data. J Hum Evol 35:647–665.

Valeri CJ, Cole TM, Lele S, Richtsmeier JT. 1998. Capturing data from three-dimensional surfaces using fuzzy landmarks. Am J Phys Anthropol 107:113–124.

Vannier MW, Marsh JL, Warren JO. 1984. Three dimensional CT reconstruction images for craniofacial surgical planning and evaluation. Radiology 150:179–184.

Zollikofer CPE, Ponce De Leon MS, Martin RD, Stucki P. 1995. Neanderthal computer skulls. Nature 375:283–285.

Zumpano MP, Carson BS, Marsh JL, Vanderkolk CA, Richtsmeier JT. 1999. Three-dimensional morphological analysis of isolated metopic synostosis. Anat Rec 256:177–188.